A Three-Dimensional Numerical Simulation of Splitting Severe Storms on 3 April 1964

ROBERT B. WILHELMSON

University of Illinois, Urbana, IL 61801

JOSEPH B. KLEMP

National Center for Atmospheric Research,[1] Boulder, CO 80307

(Manuscript received 17 December 1980, in final form 30 March 1981)

ABSTRACT

A three-dimensional numerical storm model is used to investigate the observed splitting of several reflectivity echoes on 3 April 1964 in Oklahoma. Representative soundings from this day exhibit a nearly one-directional environmental wind shear vector and the presence of strong low-level wind shear. In the numerical simulation an initial cloud splits into two long-lived rotating storms, one that moves to the left of the mean winds and the other to the right. The left-moving storm develops more slowly than the right-moving one due to the deviation of the environmental wind hodograph from a straight line below 1 km. Further, the left mover eventually splits. Convergence induced by the cold, low-level storm outflow plays a major role in the development of both the first and second splits. However, the second split appears to be dynamically different than the first as the left-moving updraft remains essentially unchanged while a new updraft forms immediately adjacent to it. Because of the different propagational characteristics of the new storm it separates from the left mover. As the left- and right-moving storms move apart, new clouds develop in between them along an expanding cold outflow boundary. In this manner the evolving storm configuration becomes similar to that of a squall line, but has evolved from a single convective cell in the absence of imposed convergence. A comparison of the simulation with observed reflectivity and surface data reveals sufficient similarity to suggest that the explanations for the model storm development also may apply to some of the observed events.

1. Introduction

Radar observations indicate that the development of severe convective storms is sometimes associated with elongation and splitting of an initial radar reflectivity region into two parts that separate in time. The storms associated with the two reflectivity regions can produce damaging winds, large hail and tornadoes. The well-known Union City tornado that occurred on 24 May 1973 was generated by such a splitting storm (Brown).[2] Bluestein and Sohl (1979) discuss another case of splitting observed in Oklahoma in 1977 while Burgess, Lemon and Achtemeier[3] summarize over 25 additional cases. Among those listed by them was a storm that developed in Texas and moved into Oklahoma on 3 April 1964. This storm was unusual in that one of the echoes that formed through splitting subsequently split again.

The behavior of the radar echoes in the different splitting storms is similar to that of the precipitation field in three-dimensional storm simulations with strong wind shear discussed by Wilhelmson and Klemp (1978) and Schlesinger (1978). In these simulations a single cloud develops from an initial impulse in an otherwise horizontally homogeneous environment. In time the rainfield elongates in the direction perpendicular to the wind shear vector and eventually splits in two. The storms develop persistent structures in which the updrafts and the precipitation-induced downdrafts support one another. These long-lived storms, commonly known as supercells, differ in a mirror image sense in that one moves to the right of the mean environmental winds with a cyclonically (counterclockwise) rotating updraft and the other moves to the left with an anticyclonically (clockwise) rotating updraft. Right-moving storms are much more frequently observed than left-moving ones and an important reason for this is that the frequently observed clockwise turning of the environmental wind shear vector favors development of the right mover (Klemp and Wilhelmson, 1978b).

In the simulations reported in Wilhelmson and Klemp (1978) we investigated the sensitivity of splitting to the strength and vertical distribution of the

[1] The National Center for Atmospheric Research is sponsored by the National Science Foundation.

[2] Brown, R. A., 1976: The Union City, Oklahoma tornado of 24 May 1973. NSSL Tech. Memo. ERL NSSL-80 [NTIS PB-269443-AS].

[3] Burgess, D. W., L. R. Lemon and G. L. Achtemeier, 1976: Severe storm splitting and left-moving storm structure. The Union City, Oklahoma tornado of 24 May 1973, R. A. Brown, Ed., NSSL Tech. Memo. ERL NSSL-80, 53–66. [NTIS PB-269443-AS].

0022-4928/81/081581-20$09.00

vector shear of the environmental wind. These simulations suggest that strong vertical shear near cloud base is necessary for splitting of an initially isolated cloud into two self-sustaining storms. Strong shear near cloud base is also observed in the environment of many documented splitting storms. Some examples of vertical shear between 1 and 2 km MSL for Oklahoma storms include 13×10^{-3} s^{-1} for the composite environmental hodograph of 3 April 1964 shown by Charba and Sasaki (1971), 9×10^{-3} s^{-1} for the Union City storm hodograph of 24 May 1973 given by Lemon *et al.* (1978), and 10×10^{-3} s^{-1} for the composite hodograph of 19 April 1972 displayed by Brown *et al.* (1973).

In our earlier simulations the environmental wind shears of 5 to 7 $\times 10^{-3}$ s^{-1} were somewhat weaker than those just mentioned. In addition, the simulations were made using an idealized, conditionally unstable sounding designed to restrict the cloud-top height to <9 km. This allowed us to limit the depth of the integration domain to 10 km in order to hold down computer requirements. Simulated updrafts and downdrafts were correspondingly weaker than commonly observed in supercells. However, the many qualitative similarities with observed splitting storms encouraged us to proceed to simulate several individual cases. Two of the storms we selected to simulate were the severe tornado producing storms that occurred in Oklahoma on 3 April 1964 and 24 May 1973. Sounding and reflectivity data were available for these splitting storms and strong low-level shear was present as previously indicated. Simulations for both of these cases resulted in left- and right-moving supercells as observed. In this presentation we shall investigate the 3 April 1964 storms in which the left mover also was observed to split. The second split appears to be different in character than the original one and analyzed surface mesonetwork data was available for comparison during it.

In simulating a specific storm our intent is to gain a better understanding of the dynamics of that type of storm. In the simulations to be presented we initialize the model with a representative vertical sounding for the observed storm environment. No account is taken of horizontal changes due to synoptic or mesoscale disturbances or to the earlier presence of clouds which could influence storm development and propagation. Further, the convection is initiated by specifying a single axisymmetric thermal. Thus, the simulated storm should be regarded as an internally consistent depiction of storm development and insofar as it compares with observations it can be used to provide us with physical insight into the observed events. The sensitivity of this development to variations in the sounding and to the model formulation have been investigated and will be reported in a future paper.

The observed development of storms on 3 April 1964 is reviewed in Section 2 and the associated environmental conditions are discussed in the following section. Modifications of the Klemp-Wilhelmson (1978a) storm model are described in Section 4 along with model initialization procedure. In Section 5 the model results are presented and related to observed events. This analysis focuses on the following aspects of the overall model development: the initial split, the storm structure subsequent to splitting, the secondary splitting of the left-moving storm and finally the eventual development of a line of storms. Concluding remarks follow in Section 6.

2. An observational overview

On the afternoon of 3 April 1964, scattered severe thunderstorms developed throughout Oklahoma. Severe winds and hail caused considerable crop and property damage and several tornadoes occurred. Both Fujita and Grandoso (1968) and Charba and Sasaki (1971) have presented pictures of storm movement on this day and the associated evolution in storm reflectivity. The main storm tracks of interest are displayed in Fig. 1a, which has been adapted from some of Fujita's unpublished figures, from the original radar film, and from Charba and Sasaki (1971). The associated 12 dBZ reflectivity contours at 0° elevation also are shown by alternating solid and dashed contours at about half-hour intervals. The tracks pass through maximum reflectivity centers denoted by the dots.

The first echo develops about 1330 along a dry line between Abilene and Wichita Falls, Texas (all times referred to are Central Standard Time). By 1400 this echo is elongating and by 1428 has split in two. Although most of the reflectivity field does split, the track of the storm moving toward the north is not connected to the original one because the maximum reflectivity region (>30 dBZ) does not appear to elongate and split. Rather, a distinct new reflectivity maximum occurs just to the northwest of the original one. The northward-moving cell is labeled L and the northeastward moving one R. The L and R indicate that the associated storms are moving to the left and right of the mean winds below 7 km. In describing the updrafts of these storms both Fujita and Grandoso (1968) and Charba and Sasaki (1971) emphasized the anticyclonic (clockwise) rotation in L and cyclonic (counterclockwise) rotation in R based on analysis of surface data and movement of small radar echo elements.

During the first split R had a noticeably greater maximum reflectivity than L and subsequently produced 3.5 inch hail and a tornado near Wichita Falls at 1510. This tornadic storm killed seven people, injured 111 people and caused $15 million in damage. After 1558 several new storms developed between L and R in a region of previous convection. These new

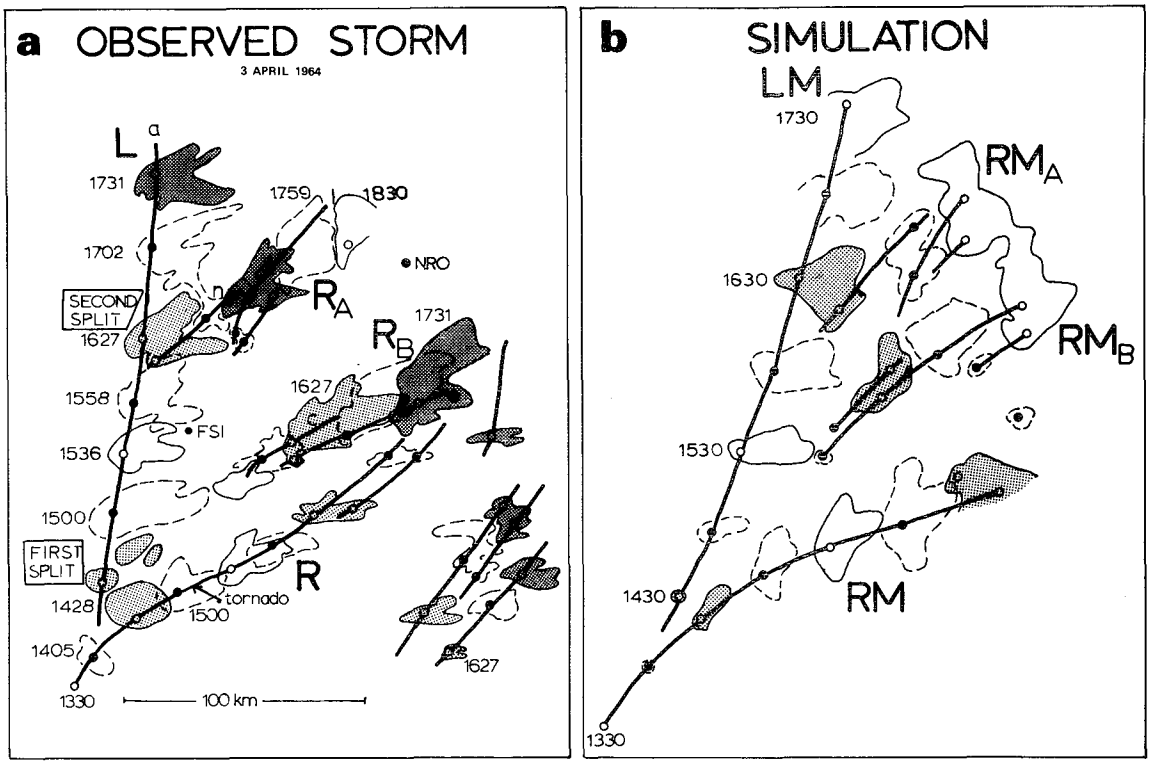

FIG. 1. The (a) observed and (b) modeled storm development on 3 April 1964. Observed reflectivities > 12 dBZ at 0° and modeled rainwater contents > 0.5 g kg^{-1} at $z = 0.4$ km are enclosed by alternating solid and dashed contours about every 30 min. Maxima in these fields are connected by solid lines. The storms are labeled and at several times the contoured regions are stippled for better visualization of the storm development. Labels for the modeled storms are the same as the corresponding observed storms except for the inclusion of M. The scale shown in (a) applies in (b).

cells formed an echo mass labeled R_B that did not appear to have split off of R as Fujita and Grandoso (1968, Fig. 2) indicated. As these cells grew, additional ones formed to the southeast of R while the tracks of the R and R_B echoes began to converge. The growth and disappearance of other reflectivity maxima occurred during this time but are not shown in Fig. 1a.

As storm L propagated toward the north it appeared to split ~30 km northwest of Fort Sill (FSI). After this second split, storm L continued to move northward with little change in direction or speed and produced 3.5 inch hail after 1700. The new echo mass denoted by R_A, however, moved to the northeast, growing and propagating by discrete development of new reflectivity cells to the southeast. The letters on the cell tracks correspond to those used by Charba and Sasaki (1971, Fig. 3). The R_A storm eventually produced hail of about 1.75 inch diameter after 1800 and subsequently a tornado funnel was sighted. The development of successive cells in R_A, coupled with little change in the propagational behavior of the cells during this split, suggests that the associated dynamics were different than for the earlier split at 1400.

3. The storm development and its relation to environmental conditions

The storms on 3 April 1964 formed in a conditionally unstable environment as illustrated in Fig. 2a which is based on the Fort Sill (FSI) sounding at 1600 obtained from Fujita (private communication) and also shown by Charba and Sasaki.[4] The sounding was taken when storm L was only ~20 km to the west of FSI. Consequently, the lowest kilometer of the FSI sounding was modified for use in the model simulation because it appeared to have been altered by storm L. The modifications were based on surface data available during the split of storm L which occurred about one-half hour after the FSI sounding was initiated.

The environmental wind profile used in the model simulation is shown in Fig. 2b and is based on a composite by Charba and Sasaki (1971) of FSI soundings at 1600 and 1720. The straight line character of the hodograph (unidirectional shear vector) above 1 km is a good approximation to the composite hodograph and was made in order to simplify our efforts aimed toward understanding modeled storm development. The actual winds obtained from Fujita (private

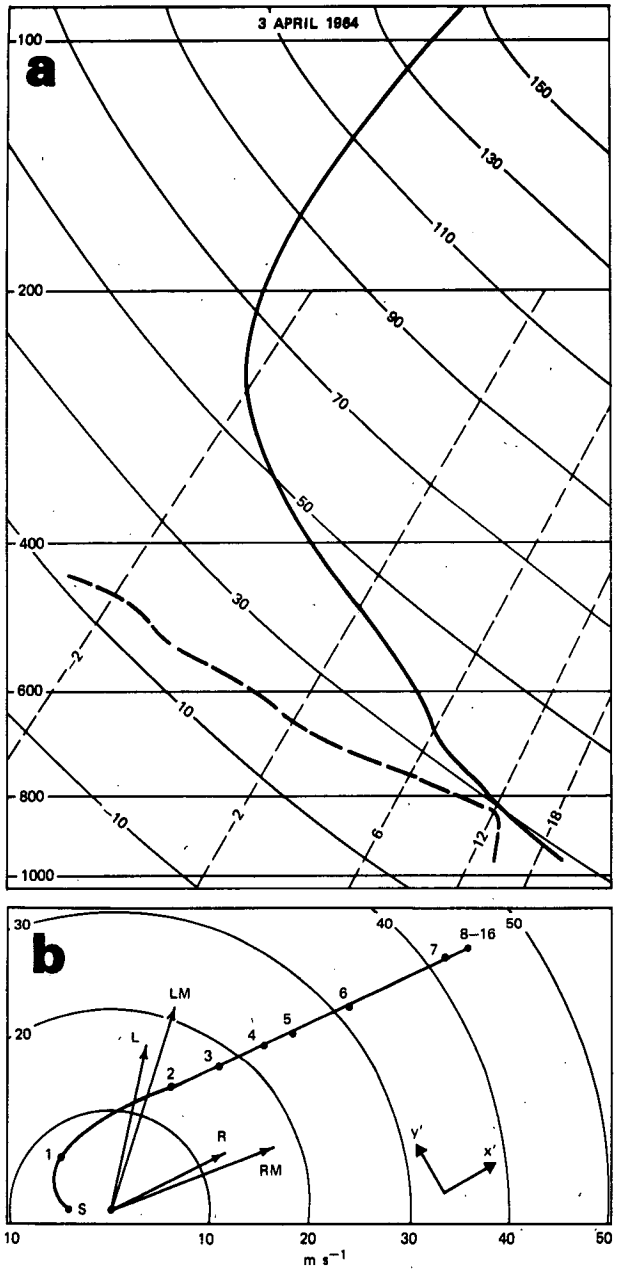

FIG. 2. (a) A skew T diagram depicting the initial temperature and moisture profiles used in the model simulation. (b) The environmental wind hodograph used to initiate the model with MSL heights labeled every kilometer. S indicates the surface value at about 380 m MSL. The average speeds of the observed storms L (1558–1702) and R (1500–1558) along with the modeled storms LM (1530–1700) and RM (1500–1630) are shown by the labeled vectors. The orientation of the x'–y' axes used in the model simulation also is displayed.

communication) indicate that the composite is most representative of the 1600 FSI sounding and that both the 1600 and 1720 hodographs are approximately straight in character above 1 km.

The straight line nature of the hodograph in Fig. 2b is similar to the one-dimensional wind-shear structure investigated by Wilhelmson and Klemp (1978). In that study, the environmental wind was specified to have components only in the east–west direction, that is, the winds describe a straight line hodograph. Surface drag and Coriolis forces were neglected and an initially isolated and axially symmetric thermal impulse grew into a storm that in its early stages moved in this east–west direction. Thus, with respect to the initial storm movement, the storm relative environmental winds were either toward or away from the storm in one direction (east–west). A similar configuration holds for any orientation of a straight line hodograph since the initial storm would move at a speed and in a direction given by some point on the hodograph line. This is illustrated in the inset of Fig. 3 which shows a straight line hodograph orientated in a similar direction to the hodograph in Fig. 2b along with an initial storm movement vector. The environmental winds relative to the initial storm motion would then lie along the hodograph line. If, for simplicity, the storm continues to move at a constant speed in the x' or hodograph direction, the development of the splitting storm and the plane of symmetry (thick line) would move as shown in

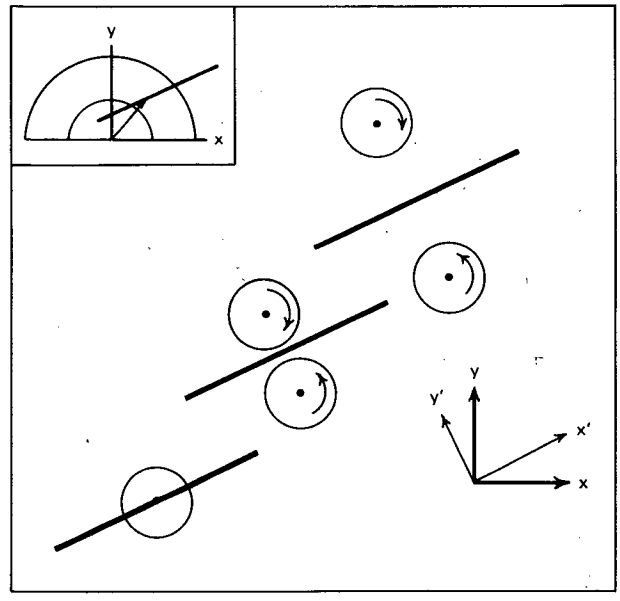

FIG. 3. The schematic development of a storm that splits in the wind field depicted by the straight line hodograph in the x' direction as shown in the inset. For simplicity the storm movement in the positive x' direction is constant. The initial cloud is mirror symmetrical about a vertical plane passing through the thick solid line and subsequent cloud development remains symmetric about this plane which moves with the storm at the speed and in the direction of the vector shown in the inset. The thick solid lines are parallel to the x' axis and to the hodograph shown in the inset. Updraft rotation is indicated by the curved arrows. Such development occurs when the environment is horizontally homogeneous and when Coriolis and drag forces are neglected.

Fig. 3. The low to mid-level rotational behavior of the updraft also is indicated.

There is a general similarity between the idealized storm motion in Fig. 3 and the observed storm development in Fig. 1a, although the observed right- and left-moving storms are not precisely mirror images in structure. The deviation of the low-level environmental wind from a straight line is an important factor that apparently causes the differential behavior. Klemp and Wilhelmson (1978b) argued on the basis of several simulations that significant clockwise curvature of a hodograph at low to mid levels will lead to limited growth of the anticyclonically rotating storm (left mover). In Fig. 2b the deviation in the hodograph from a straight line is confined to the lowest kilometer in which it turns clockwise with height. This curvature, however, is sufficient to slow down the growth of L as shown later.

Other factors also could play a role in altering mirror image symmetry of L and R. Klemp and Wilhelmson (1978b) demonstrated that in an anticyclonically rotating storm such as L the Coriolis force can suppress the development of a hook echo often associated with tornado producing storms. Horizontal inhomogeneities in the storm environment and the lack of axial symmetry of the storm during its initial formation also could be important. It is difficult to comment further on the impact of horizontal inhomogeneities encountered by the storms as they moved over 200 km because this variability is not documented in the limited data available. We also do not have much information about the early structure of semi-isolated clouds developing in strong shear. Some Doppler data of the pre-rain stage of such a cloud is available from recent observations at the National Severe Storms Laboratory; however, it has not as yet been analyzed. Thus, it is expedient to initialize the cloud somewhat arbitrarily. The use of an axially symmetric thermal, which by definition has mirror image symmetry, seems reasonable when conditional instability is strong. It is consistent with the rapid development of the initial cloud whose internal properties such as vorticity are largely governed by the interaction between the environmental wind and the dominant horizontal growth scale. The one verification we have for how we have initialized the model is the appearance of approximate mirror image symmetry in early development of the modeled and observed 3 April 1964 storms.

4. The model and its initiation

The model developed by Klemp and Wilhelmson (1978a) was used for the simulation to be discussed. The horizontally homogeneous environment in which a single storm was initiated is shown in Fig. 2. The storm was triggered by an initially specified thermal as described in Klemp and Wilhelmson (1978a). A 4°C potential temperature excess horizontally centered in the domain and vertically centered at 1.88 km above the ground was decreased to zero over a horizontal radius of 12.4 km and a vertical radius of 2.25 km.

The model domain used was 80 km × 160 km × 16.5 km with 2 km horizontal and 0.75 km vertical grid intervals. Using a 2 km horizontal grid interval is sufficient to capture the overall character of supercells as illustrated by a comparison by Klemp *et al.* (1981) which indicates good semiquantitative agreement between supercells simulated with 1 and 2 km intervals. One horizontal axis was taken in the x' direction shown in Fig. 2b which is parallel to the hodograph line between 1 and 7 km. The other axis was then taken perpendicular to it in the y' direction. Thus, true north in the model framework is 25° to the right of a vector pointing in the positive y' direction. The x'-y' coordinate system was translated at 18.5 m s^{-1} in the x' direction so that the storms which developed would remain away from the x' boundaries during the 4 h simulation. Further, the large y' dimension of 160 km was chosen in order to keep both of the split storms away from the y' boundaries for several hours.

Other model changes included the use of a 10 s large time step for physical processes of interest and a 3.3 s small time step to maintain sound wave stability. Fourth-order horizontal damping with a coefficient of $K_4 = 6 \times 10^9$ m^4 s^{-1} was used to discourage growth of numerical instability and to filter out very short wavelength modes which are improperly resolved in the model as discussed by Klemp and Wilhelmson (1978a). A second-order vertical spacial filter of the form $K_2\phi_{zz}$ was also applied for the same reason in all but the pressure equation with $K_2 = 100$ m^2 s^{-1}. The use of this value gives just slightly less damping in the vertical than in the horizontal for waves represented with eight grid points.

5. Model results and comparison to observations

a. Overall development

The model was integrated over a 4 h period and the overall development is shown in Fig. 1b. In this figure the notation is the same as that used for the observations but with the introduction of M for modeled storm. Further, the 0.5 g kg^{-1} contour of the rainwater field near the surface ($z = 0.4$ km) is shown every 30 min with alternating solid and dashed lines. In portraying the model storm development the results have been transformed from the x'-y' coordinates discussed in the last section to the physical coordinate system in which the observations are displayed. The model times shown are related to the observation times by taking 1330 as the time of model initiation in order to aid in the comparison of the

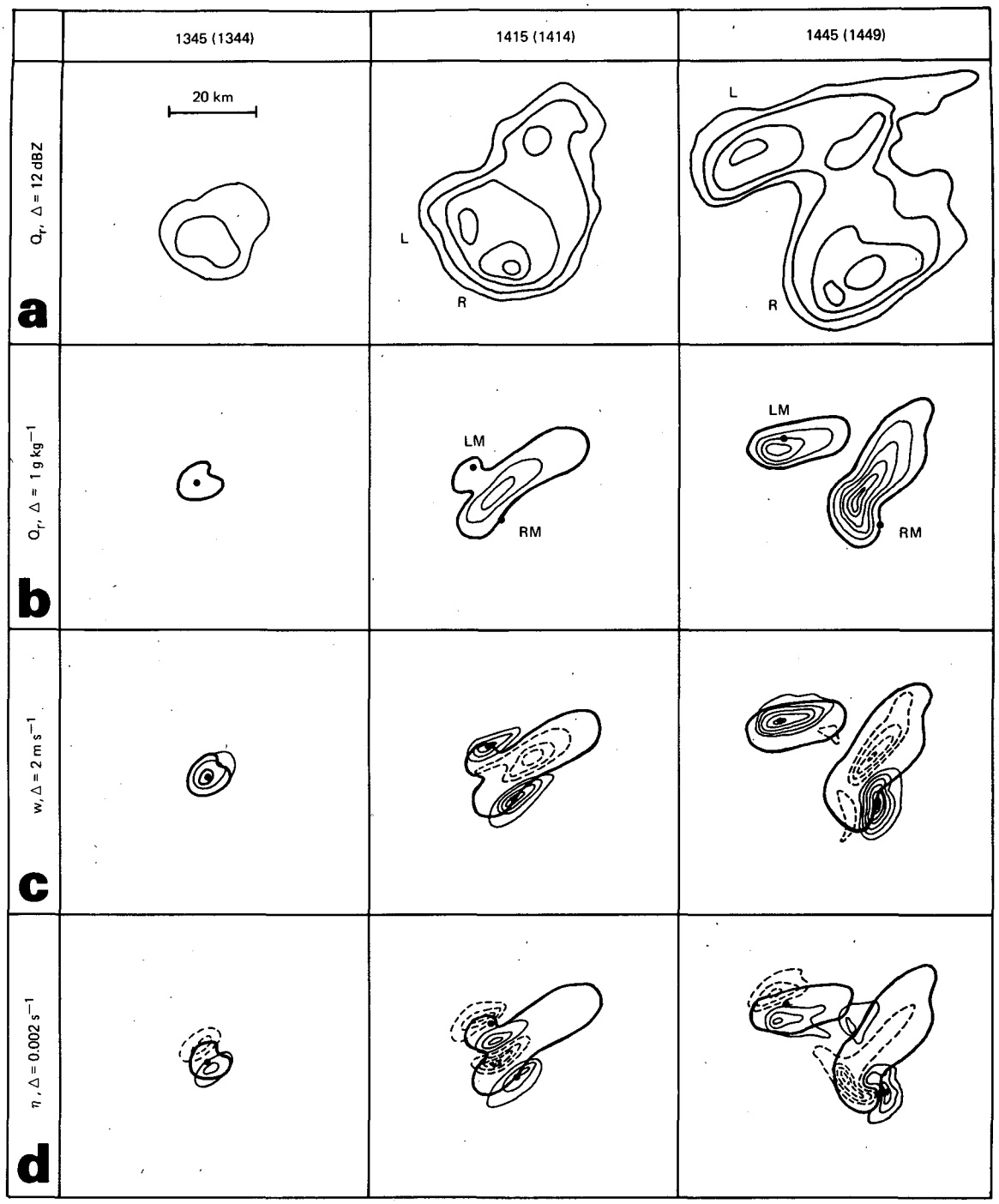

FIG. 4. (a) The splitting of the observed reflectivity at 0° with a contour interval of 12 dBZ starting at 0 dBZ. The times are indicated in the parentheses above the contours and the scale shown applies to (b), (c) and (d) as well. (b) The splitting of the modeled rainwater field at 1.9 km and at 1345, 1415 and 1445. The contour interval is 1 g kg^{-1} beginning at 0 g kg^{-1} (the thick line). (c) The splitting of the modeled updraft as in (b) with a contour interval of 2 m s^{-1} and where dashed lines are negative and the zero contour is not shown. The dots in (b), (c) and (d) denote updraft centers. (d) The vertical vorticity as in (c) but with a contour interval of 0.002 s^{-1}.

modeled and observed development. It should be kept in mind that 1330 corresponds to the appearance of the observed first echo and that a precise relationship between the two developments is not intended.

The modeled storm grows and produces precipi-

tation within 30 min. After an hour it exhibits the split behavior shown in Fig. 1b where the left-moving storm is denoted by LM and the cyclonically rotating, right-moving storm is denoted by RM. At this time the two storms have been stippled and correspond to the two observed storms at 1428 (also stippled) in that the right-moving storms are more extensive than the left-moving ones.

The model storms continue to separate in time as indicated by the storm tracks drawn through locations of maximum low-level rainwater content. The average storm speed and direction following this separation is 21.4 m s^{-1} from 197° for LM (1530–1700) and 17.4 m s^{-1} from 249° for RM (1500–1630). These motion vectors were determined from the movement of maxima in the rainwater (reflectivity) fields and are shown on the hodograph in Fig. 2b. They can be compared to the observed movement given by the vectors in that figure with speed and direction of 16.8 m s^{-1} at 192° for L (1558–1702) and 12.5 m s^{-1} at 244° for R (1500–1558). This comparison indicates a strong qualitative similarity between the observed and modeled movement, although the modeled storm propagation speeds are 4–5 m s^{-1} faster and their directions are 5° to the left of those observed.

Despite the quantitative differences in movement of the simulated left-moving storm from that observed, it also appears to split at about 1630 and the new storm that develops is denoted by RM_A in Fig. 1b. Associated with this new storm are several distinct rainwater maxima which behave qualitatively like those observed. The earliest track disappears in both situations and the general northeastward movement of the new storm is partly due to the formation of new cells to the southeast. Storm L also appears to be composed of reflectivity maxima that form to the west of old ones beginning about 1650 (see Fig. 3 in Charba and Sasaki, 1971) so that the single storm track shown in Fig. 1a actually represents the storm motion as a whole. The development of new cells in L, however, does not appear to affect the movement of L as much as new cells do in R_A. The development of these new L cells was not reproduced by the model.

New storm development denoted by RM_B occurs in between LM and RM before LM splits. This also was observed although the new storm R_B occurs closer to R, whereas RM_B occurs closer to LM. Further, the R_B storm moves in direction of R (1500–1600) while RM_B moves more in the direction of the initial storm. The origin of the RM_B storm in relationship to outflow from LM and RM will be discussed in a later section.

b. The initial split

The development of the modeled rainfield during the first split is shown in Fig. 4b at 1345, 1415 and 1445 and at $z = 1.9$ km. The contour interval is 1 g kg^{-1} beginning at 0 g kg^{-1}. As in the last section, the model results are displayed in the observational framework in order to compare against reflectivity development of 0° elevation. The reason for displaying model results at 1.9 km, rather than at the lowest model level (0.4 km) for comparison, is that the updraft and vorticity development at 1.9 km will also be discussed in order to gain insight into the differences in the behavior of the splitting storms.

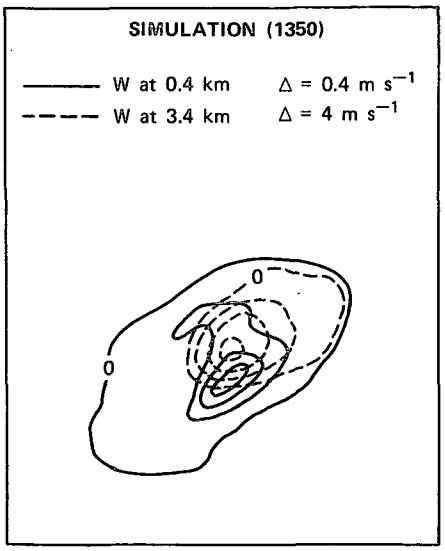

FIG. 5. The updraft at 0.4 and 3.4 km, 20 min (1350) after model initiation.

At 1345 only a small amount of rain exists at 1.9 km while 30 min later the rain field is substantial and is oriented in a southwest-to-northeast direction. A rain appendage denoted by LM is located on the northwest side of the rain region. This appendage grows and by 1445 is separate from the more intense rainfield associated with RM. Because of this delayed development the storm track for LM in Fig. 7b is not connected to the original one.

The development of the modeled rainfield at 1.9 km is generally similar to the development of the observed reflectivity field at 0° elevation shown in Fig. 4a where the contour interval is 12 dBZ starting at 0. These contours were drawn from the original radar films for times shown in parentheses. At 1344 the 12 dBZ contour is almost symmetrical about a southwest-to-northeast line through its center. This general symmetry persists as the reflectivity field broadens and two distinct reflectivity maxima form, with the one for R being somewhat stronger than the one for L as seen at 1414. A third echo also develops to the northeast for unknown reasons and remains at 1449 as L and R split. The reflectivity maxima are the same for both storms at this time, although the region of reflectivity > 24 dBZ is greater for R.

This situation persists as the storms separate completely from one another by 1500.

The development of the precipitation field both in the model and in nature are qualitatively similar to that in simulations reported by Wilhelmson and Klemp (1978) who initiated storms in an environment characterized by a straight line hodograph. However, in those simulations the split storms where symmetric in the mirror-image sense while in the case reported here the symmetry is somewhat distorted. This is further exemplified in Fig. 4c where the development of the model updraft is shown using a contour interval of 2 m s^{-1}. The zero contour, however, is not included.

At 1345 the initial updraft reaches its greatest intensity of 18 m s^{-1} at a height of 6 km and the updraft field together with the rainwater field are almost mirror images in horizontal planes ~ 1 km about a southwest–northeast plane through the updraft center. However, below 1 km the influence of the clockwise curvature in the hodograph is evident as shown in Fig. 5 at 1350. In this figure positive vertical velocity contours are shown at 0.4 and 3.4 km with contour intervals of 0.4 (solid) and 4.0 (dashed) m s^{-1}. The strongest updraft at 0.4 km is ~1.2 m s^{-1} and is situated to the south of the maximum updraft at 3.4 km. This arrangement appears to be related to the favorable low-level vertical pressure gradient that develops in the southern part of the updraft below 3.4 km due to the low-level clockwise curvature in the environmental hodograph. In contrast, an unfavorable low-level gradient acts to reduce the vertical velocity below the northern part. The development of these vertical pressure gradients is discussed by Klemp *et al.* (1981).

After 1350 a downdraft begins to form, appearing first on the upstream and downstream sides of the updraft as in the simulation reported by Schlesinger (1978). By 1415 min the downdraft has the continuous elongated appearance shown in Fig. 4c. The LM updraft associated with the rainfield appendage has about three-fourths the intensity of the one associated with RM. Further, the LM updraft decreases in strength vertically so that 1.5 km above the level shown its maximum is 2 m s^{-1} weaker while the RM updraft's is 5 m s^{-1} stronger. Higher up at 6.3 km there is no distinct LM updraft while the RM updraft maximum is 17 m s^{-1}. Thus, the LM updraft appears to have split off the lower portion of the original updraft. The upper part, however, does not split as it would in an environment described by a straight line hodograph (e.g., Wilhelmson and Klemp, 1978).

The effects of the delayed formation of LM are further exemplified at 1445 in Fig. 4c. The updraft separation is increasing while the rain field associated with LM exists primarily in the updraft and only a weak downdraft associated with it is present. The RM storm, however, has begun to take on the structure commonly associated with a right-moving storm. Half of the updraft is precipitation free and a significant downdraft exists to the north of the updraft. Furthermore, the updraft is rotating cyclonically as seen from the vorticity distribution in Fig. 4d.

The development of cyclonic rotation in the RM updraft began in the early part of the simulation when a vortex pair formed in the updraft as depicted in Fig. 4d at 1345 where the contour interval is 0.002 s^{-1} and the zero contour is not shown. In the RM updraft the vorticity is strongly influenced by stretching so that the updraft is composed primarily of positive vorticity as discussed by Klemp *et al.* (1981). In contrast, the LM updraft is composed of a vortex pair. By 1445 the vortex pair extends to 9.5 km within the updraft and due to similarity with the vortex structure at 1345 one might expect this updraft to also split; however, it does not. This is indicative of the fact that the overall airflow patterns within LM remain sufficiently similar (in the mirror image sense) to the self-sustaining ones in RM.

The ramifications of the vertical velocity and vorticity structure just discussed are clearly seen in the model precipitation field in which RM is broader and larger than RM. The observed precipitation field also exhibits such behavior, although it is not quite as obvious. The low-level clockwise curvature of the hodograph with increasing height is sufficient to account for the quantitative differences in the growth of the split storms. Further, the delayed growth of LM is related in part to the maintenance of low-level convergence at the interface between the outflow from the initial precipitation-induced downdraft and the relative environmental flow which is toward the south-southeast at 0.4 km. The importance of this is underscored by a simulation in which falling rain was not permitted. In this simulation neither a precipitation-induced downdraft nor a left-moving storm formed, although a right-moving storm did develop.

c. *Simulated storm structure two hours after initialization*

The two storms that formed out of the initial split had developed self-sustaining structures by 1530, 2 h after model initiation, and were continuing to separate from one another. In this section the structure of these storms, both of which are still well within the simulation domain, will be discussed and compared in order to investigate the differences in their structure due to the deviation of the hodograph from a straight line below 1 km. In Klemp and Wilhelmson (1978b) we showed that low to midlevel clockwise curvature could completely suppress the development of the left mover whose updraft rotates anticyclonically. However, for the hodograph given in Fig. 2b, the clockwise curvature in the x'-y' frame-

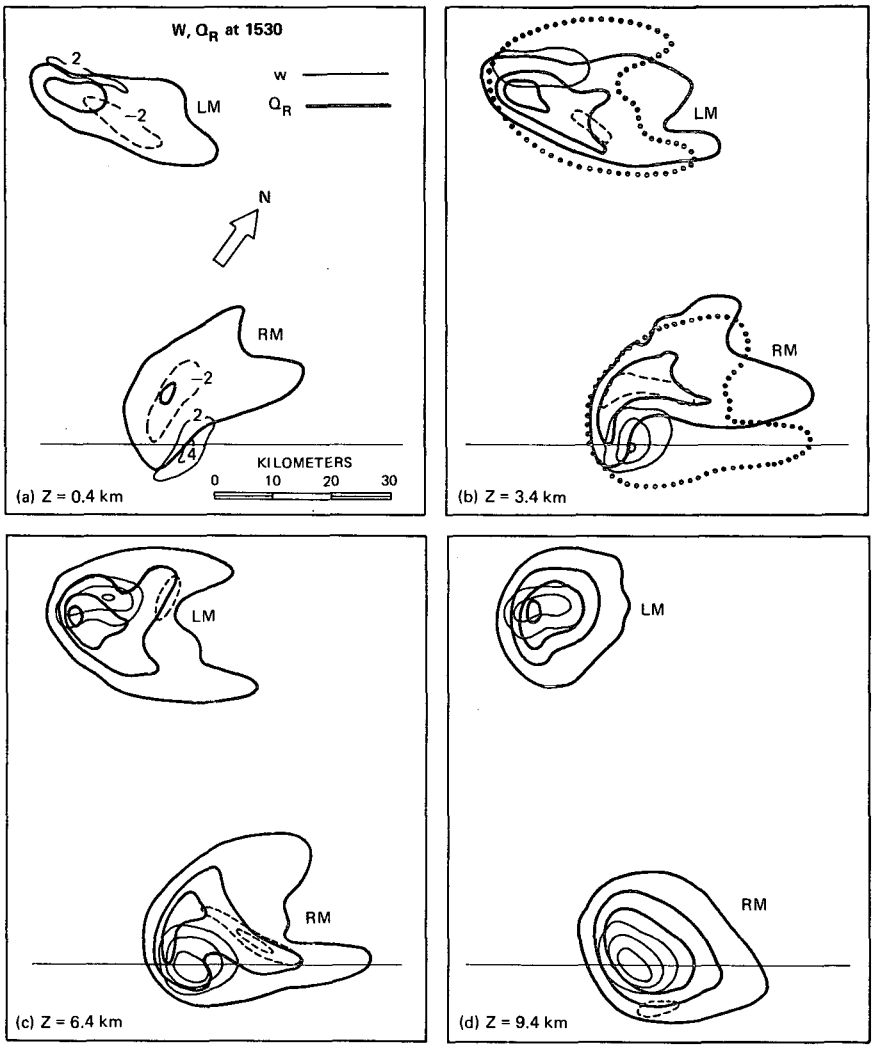

FIG. 6. The horizontal rainwater and vertical velocity structure of the modeled left-moving (LM) and right-moving (RM) storms 2 h after initialization (1530) and at (a) 0.4 km (b) 3.4 km (c) 6.4 km and (d) 9.4 km. The rainwater contours (thick solid) are 1, 5, 9 and 13 g kg^{-1}. The vertical velocities contours (thin) are labeled in m s^{-1} in (a) while those in the remaining panels are spaced 10 m s^{-1} apart except that the zero contour is not shown. The solid lines refer to updrafts and the negative ones to downdrafts. The dotted contour in (b) is the 1 g kg^{-1} contour in (c). The scale is shown in (a) along with the direction of north which is not toward the top of the page because the planes are displayed in the x'–y' framework shown in Fig. 2b. The vertical planes displayed in Fig. 8 pass through the thin horizontal lines.

work occurs below 1 km and only acts to slow down the growth of the left mover (LM). Even though the curvature does not suppress the development of LM, it is sufficient to modify the mirror image symmetry of LM and RM that would have occurred if this curvature had not been included.

The vertical velocity (thin) and rainwater (thick) contours at z = 0.4, 3.4, 6.4 and 9.4 km are shown in Fig. 6. Rainwater contours are 1, 5, 9 and 13 g kg^{-1} in this figure while north is shown by the arrow in (a) along with the spatial scale. The labeled vertical velocity contours at 0.4 km reveal that the upward motion is stronger for RM than for LM. The updrafts > 2 m s^{-1} are primarily part of the cool gust front circulation. The existence of such upward motion just behind gust fronts is well documented observationally (e.g., Charba, 1974; Goff, 1976). The downdrafts of both are about equal in magnitude, although the downdraft and precipitation regions are more extensive for RM.

Above 0.4 km the RM updraft is also noticeably stronger as shown in Figs. 6b–6d where the 0 updraft contour is not shown and the contour interval is 10 m s^{-1}. The difference between the storm max-

ima is ~11 m s^{-1} at z = 3.4 and 6.4 km and increases to 16 m s^{-1} at 9.4 km. This is indicative of the fact that LM is still growing, although during the following hour its maximum velocity only reaches ~36 m s^{-1} compared to 42 m s^{-1} for RM at the time of Fig. 6. Both occur at z = 7.9 km. The strength and height of these maxima are substantially greater than those in our previous simulations using idealized soundings (e.g., Wilhelmson and Klemp, 1978). The downdraft contours (dashed) in Figs. 6b–6d also indicate that motions associated with RM are more intense and widespread.

The rain field associated with the updrafts exhibits the opposite behavior in that the greatest water contents occur in LM. This appears to be associated with the difference in structure of the storms which is most evident at 3.4 km where a rainwater hook apparent in RM is not evident in LM. Associated with the development of the hook is an updraft whose maximum lies outside the 1 g kg^{-1} region. The cloudwater field which has zero terminal velocity encompasses a region almost identical to the main updraft at 3.4 km and thus a substantial portion exists outside the rain region. In this region, collection of cloudwater by rain is then not possible, inhibiting somewhat the overall growth of rain. This is not true for LM where rain does exist in most of the updraft and thus the rain can grow more rapidly because of collection. This view of the development of more rain in LM is substantiated by the fact that the maximum moisture and temperature deviations in both the LM and RM updrafts are almost the same at 3.4 and 6.4 km while the maximum cloudwater at these levels is substantially less in LM than in RM. It is also noteworthy that the maximum potential temperature and water vapor mixing ratios at these levels indicate regions of moist adiabatic ascent from cloud base giving evidence that entrainment has had little effect in the central part of the updraft.

The RM hook evident in Fig. 6b began to develop about an hour earlier and at 1530 lies in a region that has a strong wind component toward the south-southeast. It appears that rain falling from above and to the north is swept by it into the hook region. There is no such strong wind component in LM and no hook to the north of it. Overlying the hook is a broader rain region shown in Fig. 6c. The 1 g kg^{-1} line is also shown in Fig. 6b but by dotted contours. The overhanging character of this rain region is clearly seen and is similar to that often observed (e.g., Browning, 1965). At 9.4 km near the tropopause the rain region is more circular in character than at lower levels as shown in Fig. 6d and is nearly centered over the updraft region. There is divergent air flow in the updraft at this level which is above the level of maximum w for both storms. The temperature in the updrafts has been influenced by mixing, although perturbations are still large (e.g., up to a 9°C potential temperature deviation for RM).

The pressure and temperature fields near the surface (0.4 km) associated with the updraft and rain field just described are displayed in Fig. 7a. The pressure contours are solid lines with a contour interval of 0.6 hPa and the relative highs and lows in the horizontal plane are labeled by H and L, respectively. The potential temperature deviation contours for the environment are denoted by dashed lines 2°C apart and are labeled with their deviations from the environmental temperature, while the rain region > 1 g kg^{-1} is enclosed by the thick contour, both for discussion and for reference to Fig. 6. Low centers outside the rain region (denoted by big L's) are evident to the southeast of RM and to the north of LM. North is again displaced to the right as shown in Figs. 6a and 7b. The pressure deviation associated with the RM low is −3 hPa, about twice that associated with LM. Both lows are centered outside the cold outflow region whose boundary is taken to be the −0.5 potential temperature contour, although the low-pressure region does extend into the cold region as often observed (e.g., Lemon, 1976).

The high-pressure regions are not as well defined as the low region in that there are three relative centers associated with each storm. Two of them are relative highs and the other is a relative low. The relative lows (small L's) are located directly across the cold outflow line from the actual lows while the relative highs are located on either side of the relative lows for both storms. At this time the relative highs in RM are about of equal strength, deviating from the environment by ~1.5 hPa, while in LM the relative high to the southeast of the low is ~1.8 hPa and the relative high to the southwest denoted by the large H is ~1.2 hPa. Beyond the time shown, the high region to the southwest broadens and becomes the dominant high while the relative low region becomes smaller in extent. Further, its strength increases to match that of the low. In contrast, the relative high to the north of the RM storm denoted by the large H becomes dominant.

The reason for pointing out these differences is to note the larger variation in pressure in the high region near the surface than in the low region. These changes appear to be related to the continuously changing character of qualitatively steady-state storms. They may, in part, account for observations that delineate a distinct low in the region out ahead of the gust front but show high-pressure centers developing, decaying, and moving around in the cold outflow region (e.g., Lemon, 1976). Some observational evidence for the development of the northern high in RM after 1550 is given by Stout in Charba and Sasaki (1971, Fig. 9). Observational evidence supporting the eventual dominance of the southwestern (with respect to the low) relative high in LM will be presented in a later section. The reasons for the differences between the two storms, however, remains unclear. The dominant relative highs in the model

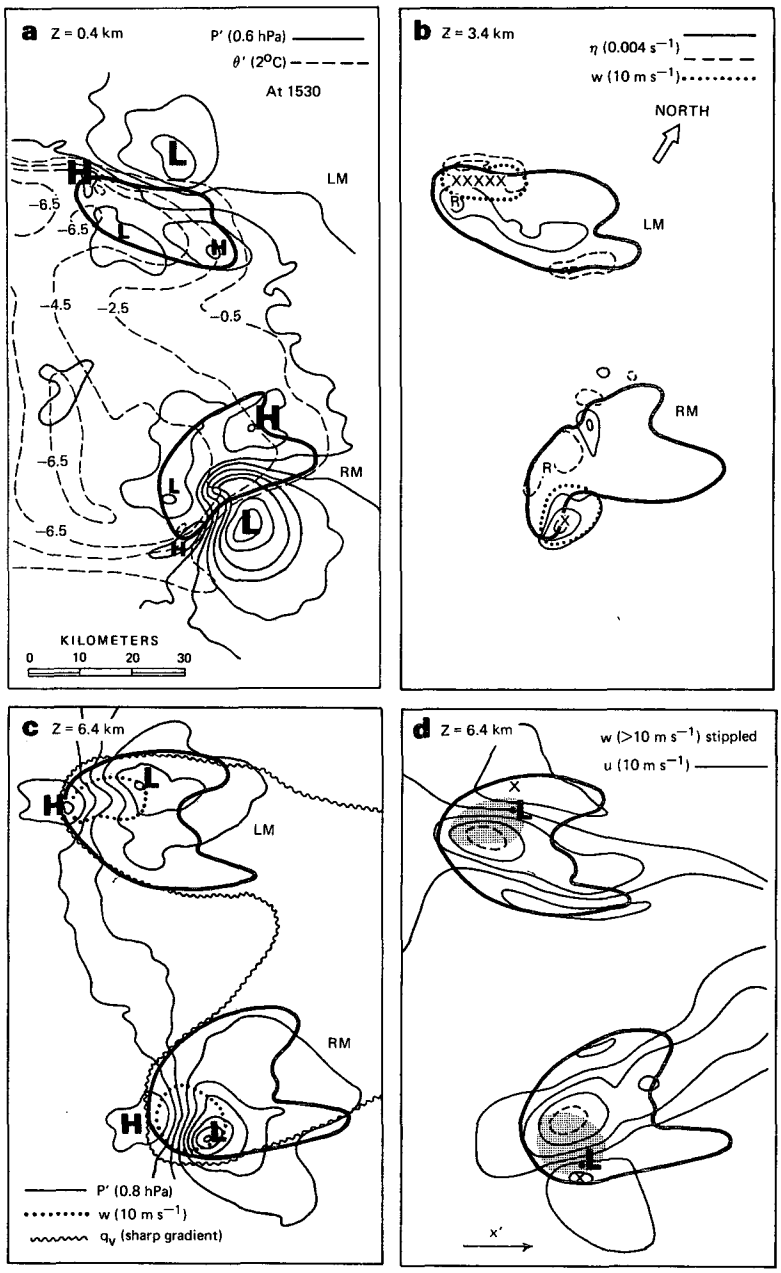

FIG. 7. Storm structure at 1530 where the thick solid line is the 1 g kg^{-1} rainwater contour at the levels shown. North is in the direction shown in (b) as in Fig. 6 and the scale for all panels is given in (a). (a) A horizontal plane at z = 0.4 km showing the modeled pressure (solid) and potential temperature (dashed) fields with contour intervals of 0.6 hPa and 2°C, respectively. The large L's denote the low centers while the small L's refer to relative lows in the cold-air region. Relative highs in the cold region are indicated by large and small H's, the large ones becoming the dominant highs after this time. (b) The vorticity (thin) contours at z = 3.4 km are shown using an interval of 0.004 s^{-1} where the zero contour is not included and dashed contours are negative. Updraft regions > 10 m s^{-1} are enclosed by the dotted contours with centers marked by the X's. The R denotes maximum rainwater locations. (c) The pressure field at 6.4 km is contoured at 0.8 hPa intervals. The locations of the maximum highs and lows are marked. As in (b), the updraft regions > 10 m s^{-1} are enclosed by the dotted contours. The wavy line indicates the location of sharp changes in the moisture field. (d) The horizontal velocity at 6.4 km in the x' direction. It is approximately relative to the storm movement in this direction and is contoured in 10 m s^{-1} intervals. The locations of several relative maxima are indicated by the X's and in shaded regions where the updraft > 10 m s^{-1}.

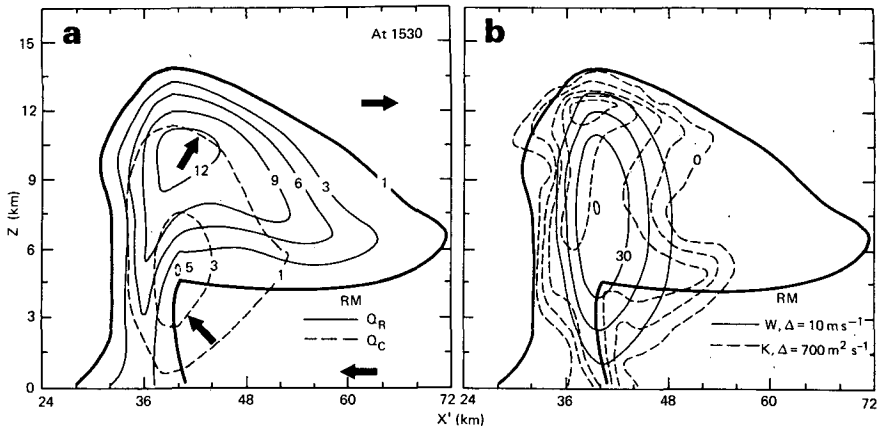

FIG. 8. Vertical planes at 1530 taken through the thin lines shown in Fig. 6. The 1 g kg^{-1} rainwater contour is shown in both panels by the thick line and only a portion of the domain in the x' direction is included. In (a) the rainwater (solid) and cloudwater (dashed) contours are labeled in g kg^{-1} and the air motion in this vertical plane is indicated by the arrows. The actual airflow to the right of the 40 km tick mark and between 1 and 6.5 km is into the page while the airflow in the remaining part of the rain region is out of the page. In (b) contours of vertical velocity (solid) and mixing coefficient (dashed) are shown with contour intervals of 10 m s^{-1} and 700 m^2 s^{-1}, respectively.

are not located in regions of maximum downdraft, although they are in the downdraft region. Thus, not only the dynamic pressure component, but also the hydrostatic and water drag components play a role in determining the locations of the maximum highs. Decomposition into these three pressure types such as that performed by Wilhelmson and Ogura (1972) or more recently by Schlesinger (1980) has not been carried out to date.

The temperature contours in Fig. 7a indicate that air within the cold outflow is as much as 6.5°C colder than in the environment. Evaporation of rain plays a significant role in cooling the downdraft air which spreads out near the surface. Temperatures in the downdrafts 1.5 km above this level are such that parcels descending adiabatically to 0.4 km would have temperatures slightly greater than the environmental temperature (rather than 5 or 6°C less).

Several other features at 0.4 km are noteworthy. The indentation of the -0.5 contour occurs more toward LM and is indicative of the greater extent to which RM is influencing surface conditions; i.e., it is more extensive and intense than LM. For both storms the low-pressure centers are not coincident with the maximum vertical velocity while the positive vorticity for RM and the negative vorticity for LM dominate in regions of upward motion. Similar pressure and vorticity relationships have been presented by Barnes (1978a,b) who analyzed mesonetwork data from two right-moving storms that occurred in Oklahoma.

The structure of the storms is further exemplified at 3.4 km in Fig. 7b where the vorticity is contoured in intervals of 0.004 s^{-1}. The dashed lines indicate negative vorticity and the zero contour is not shown. Further, the updraft > 10 m s^{-1} is enclosed by the dotted contours. The updraft in RM is rotating cyclonically with maximum positive vorticity of 0.014 s^{-1} located near the maximum updraft at position X. The LM updraft, however, has both positive and negative vorticity within it and is thus similar to that at 1445 shown in Fig. 4d. The minimum vorticity region of -0.009 s^{-1} in the elongated updraft is denoted by the X's. The fact that the maximum updraft region in LM is not dominated by negative vorticity does not affect the ability of LM to sustain itself as previously mentioned.

At 6.4 km the updraft in RM is again dominated by positive vorticity up to 0.013 s^{-1} while in LM negative vorticity down to -0.010 s^{-1} is predominant in the updraft in contrast to the situation at 3.4 km. The pressure (thin solid) at this level shows the effects of blocking with highs for both storms to the west and lows to the east near the 10 m s^{-1} updraft contours (dotted) as seen in Fig. 7c. The maximum change in pressure from low to high is 7.0 hPa for RM and 4.8 hPa for LM. The RM low is to the right of a line through the RM high in the direction of the environmental wind at this level (from left to right in the figure) while the LM low is slightly to the left.

The associated velocity in the x' (environmental wind) direction is contoured in Fig. 7d with 10 m s^{-1} intervals and is approximately relative to the two storms. The rain region > 1 g kg^{-1} is again enclosed by a thick solid line whose placement indicates that the maximum velocities occur on both sides of each storm and just inside the rain region. The largest velocities occur to the north of LM and to the south of RM. Fankhauser (1971) presents aircraft and chaff measurements which suggest a similar placement of maximum velocity for a right-moving storm. The

locations of these maximum velocities (X) are near the low-pressure centers as indicated. It is also interesting to note that the updraft region > 10 m s^{-1} in both storms includes only part of the negative velocity region. This is indicative of the importance of storm rotation as well as the upward transport of lower level momentum.

The wavy line in Fig. 7c indicates the region in which substantial moisture has been introduced by the storm circulations. It has a shape similar to that of merging anvils documented by Fujita and Grandoso (1968, Fig. 4). The parameterization of cloud substance in the model includes only the water phase and the parameterization of rain does not lead to an adequate representation of anvil conditions. Thus, the moisture field seems at this time to better portray the location of the anvil since only a small amount of cloudwater and no rain exists in much of the high moisture region.

In the previous two figures the modeled storm structure is depicted on horizontal planes. In order to get a better idea of the vertical characteristics of the right-moving storm several fields are displayed in Fig. 8 for a vertical plane through the thin lines shown in Fig. 6. The vertical scale extends from the surface to 16.5 km in Fig. 8 while the horizontal scale starts at 24 km and increases to 72 km. The actual horizontal dimensions of the model are from 0 to 80 km. In Fig. 8a the rainwater (Q_R, solid) and cloud water (Q_C, dashed) fields are shown and the contour lines are labeled (g kg^{-1}). Arrows indicating the airflow in the vertical plane are also shown. The actual airflow to the right of the 40 km tick mark and between 1 and 6.5 km is into the page while the airflow in the remaining part of the rain region is out of the page.

Much of the air entering the updraft condenses in a rain free region which is bordered on the left by a vertical wall of rain. Radar observations of some severe storms also exhibit a similar wall appearance as documented by many authors including Browning and Donaldson (1963) and Fankhauser (1971). Above the vertical wall the modeled cloud extends to ~13.5 km while RHI radar returns on 3 April indicate storm tops up to ~14.5 km. The modeled cloud is then at least a kilometer shorter than some of those observed. A precise difference in height is hard to obtain because of difficulties in relating reflectivities to model water content.

The cloud and rainwater patterns shown in Fig. 8a are generally similar to those shown by Wilhelmson and Klemp (1978, Fig. 9), although the cloud is twice as deep and the magnitudes are larger. The other quantitative difference is the gentle rather than sharp downward slope of the rainfield from the top of the cloud toward the right as is often observed. A 5–6 km descent is the reflectivity field is indicated, for example, by Browning and Donaldson (1963) and Fankhauser (1971) and a similar descent was documented on 3 April for the left-moving storm by Charba and Sasaki.[4]

The updraft associated with the water fields is contoured (thin solid) in Fig. 8b starting at 10 m s^{-1} and in 10 m s^{-1} increments. The updraft region is erect, despite the strong environmental wind shear. The maximum RM updraft occurs in this plane and is close to 40 m s^{-1}. A 2 m s^{-1} downdraft (not shown) exists in the lower portion of the rain region. A more complete three-dimensional picture of the flow field for a right-moving storm is given in Klemp *et al.* (1981). Although it is not based on this simulation, many features are similar.

The mixing coefficients determined using a prognostic subgrid energy equation are also contoured (dashed lines) in Fig. 8b. The contours begin at 0 and increase to 2800 m^2 s^{-1} in intervals of 700 m^2 s^{-1}. Significant gradients occur inside the 0 m^2 s^{-1} contour that surrounds updrafts > 10 m s^{-1}. The largest gradients occur on the upwind (left) side and at the top. This is similar to the results reported by Klemp and Wilhelmson (1978a, Fig. 7) and further emphasizes that significant physical mixing occurs almost entirely in the updraft of the storm. Little mixing occurs in the downdraft or in the boundary layer because the air is stable enough to offset any effects due to the wind shear [Klemp and Wilhelmson, 1978a, Eq. (3.12)].

The magnitudes of the mixing coefficient are noticeably larger than in Klemp and Wilhelmson (1978a). In the model these mixing coefficients are related to the subgrid-scale energy E using the relationship $K_m = c_m E^{3/2} l$, where l is the length scale defined in terms of the grid size and c_m is a constant coefficient. For the simulation $K = 700$ m^2 s^{-1} corresponds to a subgrid energy of 5.9 m^2 s^{-2} and if the energy is divided up equally into all three wind components this corresponds to a velocity of 2.0 m s^{-1}. For $K = 2800$ m^2 s^{-1} the velocity would be 7.9 m s^{-1}. Thus, in regions of large mixing the subgrid motion is substantial, but still significantly smaller the observed motions. Further, the dissipation associated with a $K_m = 2800$ m^2 s^{-1} is 0.13 m^2 s^{-3}, compared to maximum values of 0.36 m^2 s^{-3} estimated by Frisch and Strauch (1976) from Doppler-radar data for a Colorado storm. These numbers are reasonably close considering both the model and radar data approximations involved.

d. Development of the second split

After 2 h of simulation the right-moving storm (RM) proceeded to move out of the domain while the left-moving storm (LM) remained within it. Further, the LM rain field elongated and split in a man-

[4] Charba, J., and V. Sasaki, 1968: Structure and movement of the severe thunderstorms of 3 April 1964 as revealed from radar and surface mesonetwork data analyses. NSSL Tech. Memo. ERLTM-NSSL 41, 47 pp. [NTIS 183310].

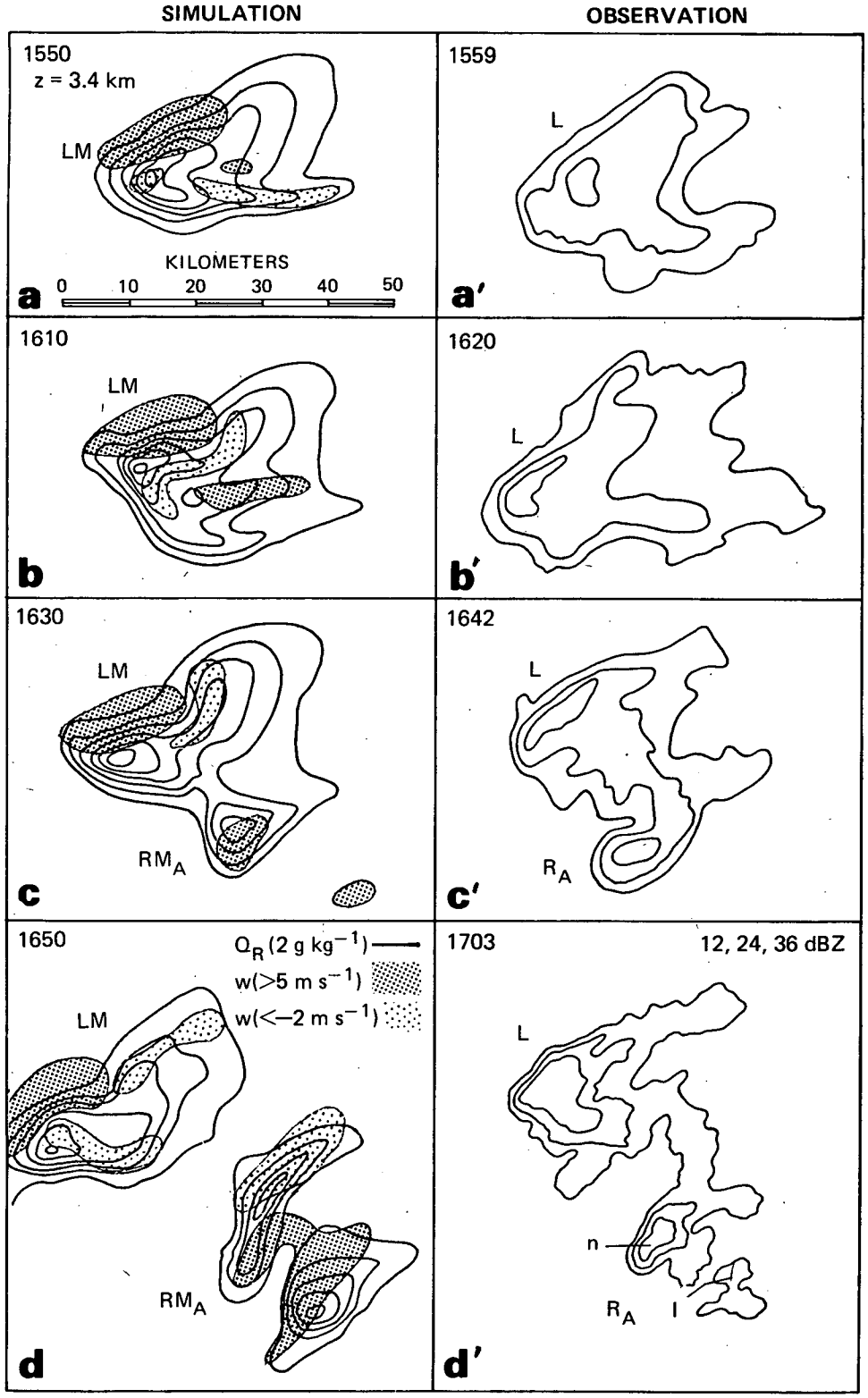

FIG. 9. The development of the simulated rain and vertical velocity fields at $z = 3.4$ km are shown every 20 min in (a)–(d). The rain field is contoured in 2 g kg^{-1} intervals starting at 1 g kg^{-1}. Vertical velocities > 5 m s^{-1} occur in the densely stippled regions while those less than -2 m s^{-1} occur in the sparsely stippled regions. The scale for all panels in the figure is shown in (a). The development of the observed reflectivity field at 0° elevation is shown in (a')–(d'). These panels are ~20 min apart as indicated by the times shown and the 12, 24 and 36 dBZ contours are displayed. The labels on the cells in (d') are the same as those in Fig. 1b.

ner similar to the observed storm L as seen in Fig. 1. This second split will be discussed in this section in order to show the similarities and differences between it and the earlier split into left- and right-moving storms.

The overall development of the second split in the model is illustrated in Figs. 9a–9d at 20 min intervals starting at 1550. Both the rain and the vertical velocity are shown at $z = 3.4$ km in the observational framework (i.e., north is toward the top of the page). The rain field is contoured in 2 g kg^{-1} intervals starting at 1 g kg^{-1}. It elongates roughly in a north–south direction from 1550 to 1620 and by 1630 two distinct rainwater maxima are quite evident. Subsequently, the rainfield splits into two parts and a third rain region appears to the southeast and becomes more intense than the split storm just to the north of it.

The modeled development resembles that observed as seen in Figs. 9a′–9d′ where 12, 24 and 36 dBZ reflectivity contours are displayed. These contours were taken from Charba and Sasaki (1971) at intervals as close to 20 min as possible. The first time selected for display was 1559, 9 min after that in the model in order that the observed sequence bear close resemblance to that modeled at 3.4 km. This model level, rather than one near the surface, is shown for discussion of the storm dynamics and we note that the general development of the modeled rainfield at this level is similar to that which occurs ~10 min later near the ground. A precise comparison of the modeled and observational time sequence, however, is not intended. Our intent is to show that the dynamical changes during the modeled split provide a plausible explanation of what happened on 3 April.

The observed reflectivities behave in a qualitatively similar manner to those modeled. The reflectivity (rain) maxima in L (LM) occur in the northwest part of the storm and a new maximum develops to the southeast as the storm elongates. By 1703 R_A has almost split away from L completely and is composed of several cells. Several of these cells are labeled and their tracks are shown in Fig. 1a. It is evident from looking at the observations that the reflectivity development in R_A at this time is complicated as a number of small cells also appear to be identifiable.

During the modeled and observed split the original storm appears to maintain its general character as it continues to move in approximately the same direction and speed as before the split. This differs from the earlier split in which an initial storm develops into two storms moving in different directions and at different speeds. The development of the second split is preceeded by the formation of a new updraft to the southeast of LM's updraft and downdraft. This is shown in Figs. 9a–9d where regions with vertical motion > 5 m s^{-1} are densely stippled and regions less than −2 m s^{-1} are sparsely stippled. The updraft associated with LM is evident at all times and this is consistent with the similar behavior of LM before and after the split. The downdraft region occurs primarily to the south and east of the updraft, with the locations of regions less than −2 m s^{-1} varying in time.

The new updraft begins to develop along the 5 g kg^{-1} rainwater contour in LM at 1550. It deepens in time and moves in a direction similar to that of the original storm at 1500. Since the structure and movement of LM is not significantly changed by the new development, the storms begin to separate. The new storm updraft rotates cyclonically and an associated downdraft begins to develop (Fig. 9d). The storm might have developed into a right mover; however, in both the model and the observations it dies out as another new cell develops to the southeast of it. The generation of cyclonic rotation in this developing storm appears to be related to its close proximity to LM since a vortex pair developed in the updraft when it occurred further away from LM in several other simulations we have made.

e. *Modeled and observed surface conditions during the second split*

In the last section we noted that the modeled second split occurred as a new updraft developed to the southeast of the left moving storm LM. The 0.4 km divergence field at 1610 associated with this new development is shown in Fig. 10a in the observational framework with a contour interval of 2×10^{-3} s^{-1}. The main convergence (C) and divergence (D) centers are marked and at this model level convergence is synonymous with upward motion and divergence with downward motion. Also, rain regions > 1 g kg^{-1} are stippled. The western convergence-divergence pair is associated with the basic self-sustaining structure of LM. Converging air feeds the updraft while descending air spreads out with maximum divergence near the region of greatest rainwater. This arrangement is accompanied by strong north-south gradients in pressure, potential temperature and water mixing ratios as seen in Figs. 10b–10d.

The solid pressure contours shown in Fig. 10b are 1 hPa apart and indicate a low to the north of LM's rain region as before (at 1530). The dashed contours differ from the neighboring solid ones by 0.5 hPa and help to indicate the high area within the rain region. The pressure difference between low and high regions exceeds 4 hPa, somewhat larger than at 1530 because of the increased strength of LM. Another significant low center to the east of RM_B rain region is also apparent in the figure. This low, coupled with the convergence center to the southwest of it, is supporting the development of RM_B.

Another convergence center occurs to the southeast of the one supporting LM. This center began to develop closer to LM's and much earlier. The new updraft associated with it deepens as the conver-

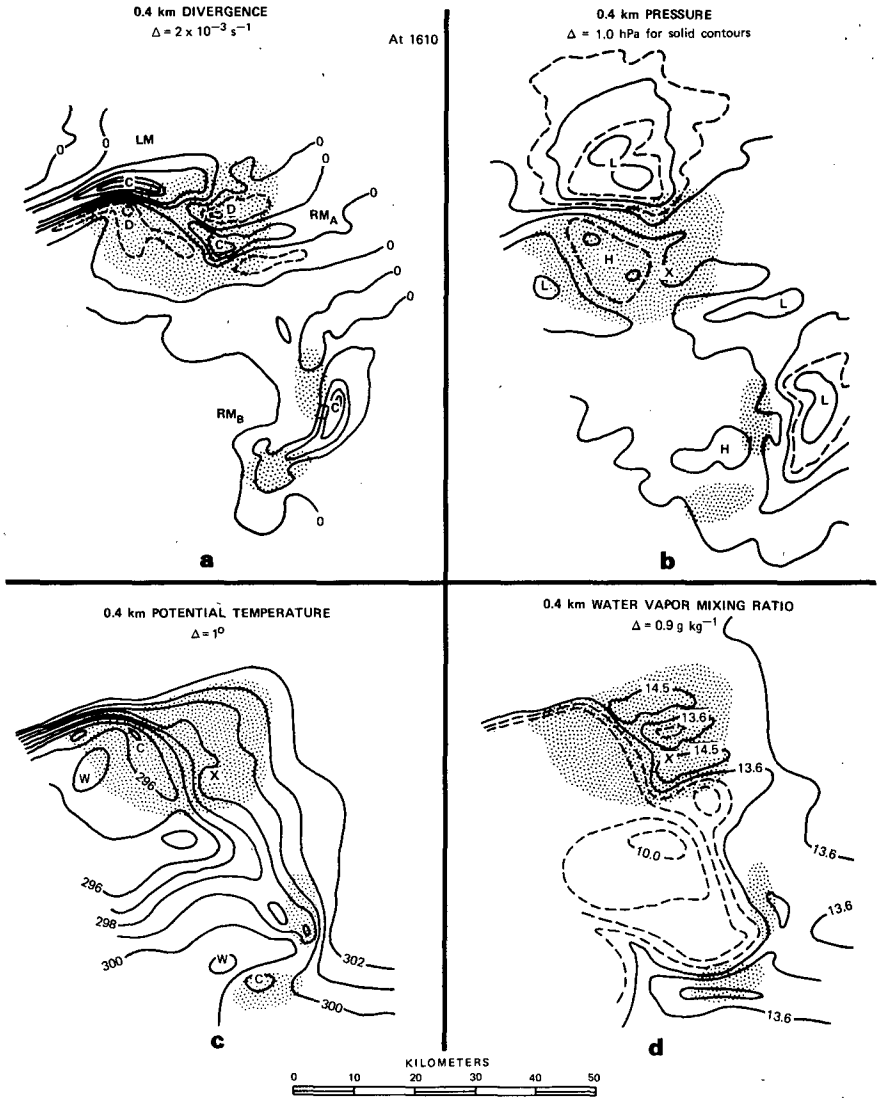

FIG. 10. Horizontal cross sections of (a) divergence, (b) pressure, (c) potential temperature and (d) water vapor mixing ratio at 1610 and $z = 0.4$ km in the model. The contour intervals are given beneath the panel titles. The C and D in (a) refer to convergence and divergence centers, the H and L in (b) refer to relative highs and lows in the horizontal plane and the C and W in (c) refer to relative cold and warm centers. The X in (b), (c) and (d) is located at the center of convergence region inside the LM's rain region. The dashed contours in (b) differ from the neighboring solid contours by 0.5 hPa. Rain regions > 1 g kg^{-1} are stippled.

gence centers separate so that by 1610 there is only a narrow band of convergence between them. At the same time a new divergence center develops in the eastern part of the rain region. Air descending in this region is unsaturated and drier than in the environment as seen in Fig. 10d where the environmental water vapor mixing ratio is 13.6 g kg^{-1}.

The new RM_A updraft differs from that associated with LM. First, it is rotating cyclonically, i.e., it is composed almost entirely of positive vorticity. Second, the equivalent potential temperature of a moist adiabat based on maximum temperatures in the lower part of the updraft is ~4°C less than for LM or RM. This is consistent with the characteristics of the relative low-level air entering the RM_A updraft (above the new convergence zone) from the east-northeast. As this air approaches RM_A with a potential temperature of 302 K it is cooled and moistened (1 g kg^{-1} evaporation gives 2.5° cooling in the model) in part by evaporation of rain falling into it. Upward movement of air near the surface ($z = 0.4$ km) also contributes to these changes since the vertical gradient of potential temperature is positive and of water vapor is negative. This latter effect is most evident in the water vapor field (Fig. 10d) and also appears in the potential temperature field (Fig. 10c). For ref-

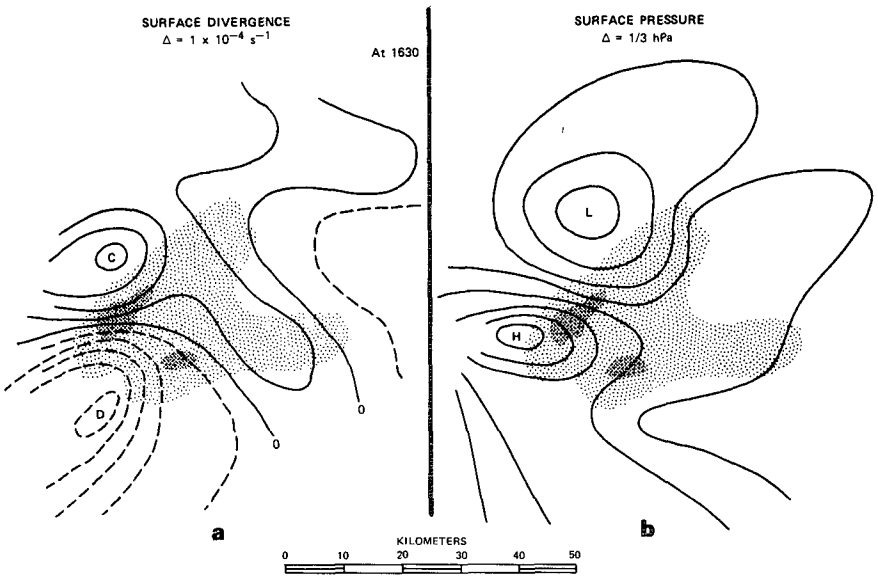

FIG. 11. Horizontal cross sections of (a) surface divergence and (b) surface pressure at 1630 which have been adapted from the mesonetwork analysis of Charba and Sasaki (1971). The 12 (light) and 36 (heavy) dBZ regions are stippled while the letters and contour intervals are described in Fig. 10.

erence, the X in these figures denotes the location of maximum convergence. Because of these factors the air rising in RM_A's updraft needs to be lifted to ~2.5 km before it reaches its level of free convection, rather than ~1.2 km for LM or RM. This occurs as air from the east-northeast is forced upward in the convergence zone just to the east of the sharp horizontal gradients in potential temperature and water vapor.

It is interesting to note that in Fig. 10c cool air occurs not only to the east of the LM and RM_B rain regions, but also in between them. To the east of the 1 g kg^{-1} rain regions the cooling is probably due to evaporating rain as mentioned in the previous paragraph. In addition, a significant amount of this cool air occurs to the east of the wind shift line which is situated in the rain region near the 299 K contour line. In between the rain regions the cool air can be accounted for by movement of air to the south-southeast which has been cooled and moistened by evaporation when it was located to the east of LM. The complicated structure surrounding and between the storms makes this process difficult to show clearly without further detailed analysis.

Surface data during the actual split of storm L have been analyzed by Charba and Sasaki (1971). During the 1964 NSSL spring program 47 stations were spaced 18–27 km apart. Because of the large separation between stations Charba and Sasaki assumed the storm parameters were stationary for up to 20 min in order to convert time variations into spacial variations. Despite the fact that R_A was forming during analysis times, several model features are evident. The divergence field at 1630 and at the surface is shown in Fig. 11a with a contour interval of 10^{-4} s^{-1}, 20 times smaller than in the model. The 12 (light) and 36 (heavy) dBZ regions are stippled [Charba and Sasaki used 6 and 30 dBZ] and indicate that R_A is identifiable. Maximum convergence to the northwest of the rain region is evident, while maximum divergence occurs to the southwest of it. The

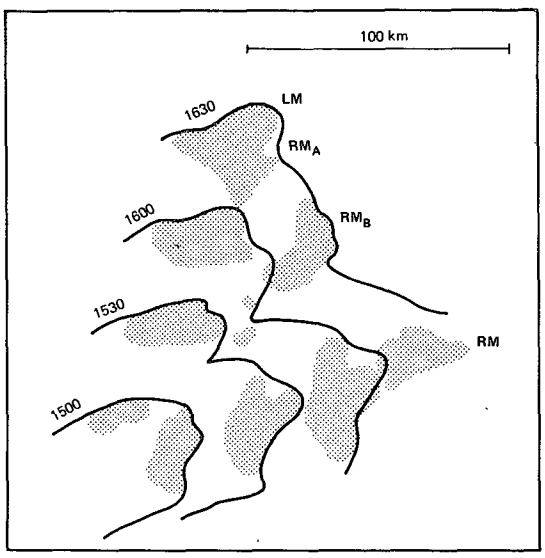

FIG. 12. The progression of the modeled cold outflow boundary in time at z = 0.4 km, where the −0.5°C potential temperature contour is indicated by the thick solid lines. Regions enclosing rainwater > 0.5 g kg^{-1} are stippled.

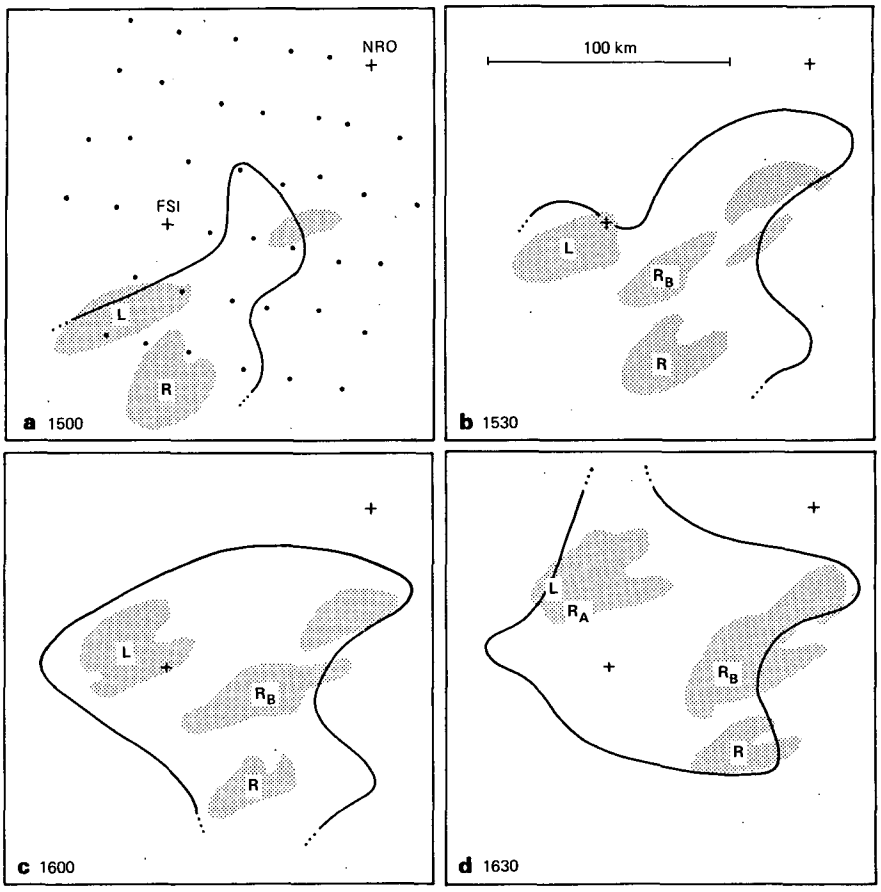

FIG. 13. The development of cold air regions at the surface on 3 April 1964 is shown. At the times indicated the solid lines enclose regions in which the potential temperatures are at least 1.5°C colder than the corresponding maximum potential temperature after 1430. Smoothed reflectivity regions > 0 dBZ are stippled.

difference between centers is 9×10^{-4} s^{-1}, whereas in the model it is 120×10^{-4} s^{-1}. The factor of 10 difference may be due largely to resolution as grid point separation in the model is 2 km and station separation is about 10 times greater. Why the maximum divergence would occur outside the downdraft-rain region is unclear. It is possibly an artifact of the course resolution because at 1645 the analysis of Charba and Sasaki indicates that it is within the rain region. What is evident, however, is the existence of a band of convergence through the rain region in similar fashion to that modeled and shown in Fig. 10a. This band of convergence also was found by Charba and Sasaki at 1615, before the reflectivity maximum associated with R_A had appeared, and at 1645.

The observed pressure field at 1630 indicates a well-defined low and high as seen in Fig. 11b. The difference between them is 2.3 hPa, about one-half that modeled. A distinct high-pressure region was not evident at 1615 while at 1645 it is evident within the maximum reflectivity region. This variability in behavior together with that of the maximum divergence region may indicate that the analysis suffers from the course network of observing stations in relation to the scale of the storms.

f. Modeled and observed line development

One of the intriguing aspects of our model simulation and observed events on 3 April is the development of a line of clouds from a single cloud. This mesoscale development from a single cloud is quite clear in the model as seen in Fig. 1b and occurs apart from any initial mesoscale forcing. As the initial storm splits a region of cold air persists between the storms and is intensified by the development of RM_A and RM_B. This is shown at $z = 0.4$ km in Fig. 12 where the -0.5°C potential temperature perturbation contour is drawn in the observational framework at half-hour intervals starting at 1500. Also included are stippled regions in which the rainwater content is >0.5 g kg^{-1}. The cool region to the west of the temperature contour expands with the splitting

storms and might have also split if RM_B had not appeared at 1600 along the cold outflow boundary. By 1630 RM is moving out of the integration domain and the separation of the −0.5°C contour from the RM's rain region apparently results from problems near the boundary.

It is important to recognize that over a 4 h period the boundary conditions control to some degree what happens within the integration domain. Clark (1979) found that the boundary conditions we are currently using led to a steady growth of the horizontally averaged vertical velocity in a simulation of multiple cells using an anelastic cloud model. Values at some levels exceeded 2 m s^{-1} after 5000 s and Clark argued that this was due to overdevelopment of the large-scale circulation induced by the clouds within the domain. The large values may have resulted from his use of an intrinsic gravity wave speed of $c^* = 45$ m s^{-1}. In the simulation presented in this paper $c^* = 30$ m s^{-1} and average values did not exceed 1.0 m s^{-1} at any level for the 4 h of integration. Tripoli and Cotton (1980) found similar results, but for only 1 h simulations. Values at most of the cloud levels grew during the first 2.5 h of the simulation as more convection developed. Then values oscillated until the last half hour of the simulation where they grew again. The growth during the first few hours was associated with increased convective development. In turn, more precipitation formed and more reached the ground. However, because of the high vertical shear in the environment only ~20% of the water that condensed ever reached the ground. This is common for observed storms occurring in strong shear (Browning, 1977), although the method of computation differs.

An analysis of the observations similar to that shown in Fig. 12 is complicated because the temperature within the region in which the storm propagated was not constant. It ranged from ~21°C in the northeastern region to 26°C in some western and southern areas. Furthermore, RM_B formed in a region affected by a previous storm. Thus, it is most meaningful to look at regions in which the temperature drops, rather than at temperature contours. The contours in Fig. 13 enclose regions in which the temperature at a point is at least 1.5°C colder than its maximum, the latter occurring sometime after 1430. This was determined using the surface station data provided for us by Dr. Fujita (personal communication). Further, the smoothed reflectivity regions greater than 0 dBZ are stippled.

The influence of the splitting storms L and R, as well as the storm to the northeast, is evident at 1500 in Fig. 13a. The cool region elongates in a northwest to southeast direction while L and R separate (Figs. 13b and 13c). As the storm system moves off to the northeast the temperature of the air far behind the storm begins to increase (Figs. 13c and 13d). The cool region is in part linked with the spread of cool downdraft air near the surface associated with old and new storms. It probably is also affected by a reduction in surface heating due to anvil formation.

Although the observed line development is more complex than that modeled, a cool air region does exist along and behind (to the southwest of) the line in both cases despite the differences in separation of storms. This, coupled with the other similarities previously discussed, indicates that both modeling and observational analysis can be used constructively to better understand storm dynamics.

6. Concluding remarks

The research presented in this paper is an extension of that reported by Wilhelmson and Klemp (1978) to include the simulation of an observed splitting storm that occurred on 3 April 1964. In the model used (Klemp and Wilhelmson, 1978a) the microphysical interactions are treated with only two categories of water and the subgrid turbulence is parameterized with the aid of a prognostic equation for subgrid-scale kinetic energy. A relatively coarse 2 km horizontal and 750 m vertical grid interval are adopted and a representative environmental sounding is used throughout the model domain. Despite these and other simplifications made in developing and initializing the model, the early cloud that forms splits into two long-lived storms as observed.

This split into two self-sustaining storms is similar in general character to those that occurred in an environment described by a one-directional wind-shear vector as reported by Wilhelmson and Klemp (1978). This similarity is related to the presence of strong low-level shear in both cases. In Wilhelmson and Klemp (1978) the two split storms were symmetric in the mirror image sense. However, in the simulation reported here the two storms are only qualitatively symmetric after several hours of integration due to the clockwise turning of the hodograph with increasing height below 1 km as seen in Fig. 2b. If the hodograph line had been completely straight the split storms would have been symmetric.

One effect of the low-level turning in the wind is the slower development of the left-moving storm (LM) due in part to an unfavorable low-level vertical pressure gradient. Convergence along the gust front, however, promotes the growth of the LM updraft. Without this convergence the left-moving storm would decay as confirmed by a simulation in which rain was not allowed to form. There also are quantitative differences in character between the left- and right-moving storms due to the turning of the low-level wind. For example, the updraft in the left mover is weaker than in the right mover when both are fully developed. Further, the updraft from cloud base

to 5 km is composed of a vortex pair in contrast to the predominantly cyclonic rotation (positive vorticity) that exists in the right-moving updraft. Despite these differences both the storms are long-lived because the basic air flow and rain flow patterns that develop within them are quite similar in the mirror image sense.

About 2 h after the split of the initial storm into right and left moving ones a second split occurs. During this split a new storm (RM_A) is initiated by convergence within the outflow region of LM along a wind shift line. As RM_A develops and rain forms within it, the LM rainfield appears to elongate and eventually split because of the different propagational characteristics of RM_A. During and after the split LM maintains its structural and propagational characteristics.

At the same time that RM_A is growing, new convection also develops along the cold outflow boundary between LM and RM. The resulting overall structure of the new and old storms is similar to that of a squall line. This line develops from a single storm apart from any mesoscale forcing. Severe squall lines do not usually form in this way, although they could as demonstrated from the model and observational analyses.

There are many uncertainties in integrating the model for 4 h. Despite these and the complexity of the observed storm development, some qualitative similarities do exist between models and observed rainwater (reflectivity) and surface features on 3 April 1964 during the first and second splits. This does not imply that the model can be used to predict storm development at this time. Rather, it implies that under certain circumstances, modeling efforts and observational analyses can be combined to gain a better understanding of storm development and structure.

Acknowledgments. The authors wish to thank Ms. K. Garrelts for typing the manuscript and Mr. Kelvin Droegemeier for comments on the manuscript. Further, we would like to thank Dr. Ted Fujita for lending us his records on the observed storm development. The model simulation was performed on the CRAY-1 computer at the National Center for Atmospheric Research which is supported by the National Science Foundation. This work was supported by the National Science Foundation under NSF Grants ATM 78-01010 and ATM 80-11984, and by NOAA under Grant NA80-RAD0005, R59.

REFERENCES

Barnes, S. L., 1978a: Oklahoma thunderstorms on 29–30 April 1970. Part I: Morphology of a tornadic storm. *Mon. Wea. Rev.*, **106**, 673–684.

——, 1978b: Oklahoma thunderstorms on 29–30 April 1970. Part II: Radar-observed merger of twin hook echoes. *Mon. Wea. Rev.*, **106**, 685–696.

Bluestein, H. B., and C. J. Sohl, 1979: Some observations of a splitting severe thunderstorm. *Mon. Wea. Rev.*, **107**, 861–873.

Brown, R. A., D. W. Burgess and K. C. Crawford, 1973: Twin tornado cyclones within a severe thunderstorm: Single-Doppler radar observations. *Weatherwise*, **26**, 63–71.

Browning, K. A., 1964: Airflow and precipitation trajectories within severe local storms which travel to the right of the winds. *J. Atmos. Sci.*, **21**, 634–639.

——, 1965: Some inferences about the updraft within a severe local storm. *J. Atmos. Sci.*, **22**, 669–677.

——, 1977: The structure and mechanisms of hailstorms. *Hail: A Review of Hail Science and Hail Suppression*, G. B. Foote and C. A. Knight, Eds., *Meteor. Monogr.*, No. 38, Amer. Meteor. Soc., 1–43.

——, and R. J. Donaldson, Jr., 1963: Airflow and structure of a tornadic storm. *J. Atmos. Sci.*, **20**, 533–545.

Charba, J., 1974: Application of gravity current model to analysis of squall-line gust front. *Mon. Wea. Rev.*, **102**, 140–156.

——, and V. Sasaki, 1971: Structure and movement from severe thunderstorms of 3 April 1964 as revealed by radar and surface mesonetwork data analysis. *J. Meteor. Soc. Japan*, **49**, 191–213.

Clark, T. L., 1979: Numerical simulations with a three-dimensional cloud model: Lateral boundary condition experiments and multicellular severe storm simulations. *J. Atmos. Sci.*, **36**, 2191–2215.

Fankhauser, J. C., 1971: Thunderstorm-environment interactions determined from aircraft and radar observations. *Mon. Wea. Rev.*, **99**, 171–192.

Frisch, A. S., and R. B. Strauch, 1976: Doppler radar measurements of turbulent kinetic energy dissipation rates in a northeastern Colorado convective storm. *J. Appl. Meteor.*, **15**, 1012–1017.

Fujita, T., and H. Grandoso, 1968: Split of a thunderstorm into anticyclonic and cyclonic storms and their motion as determined from numerical model experiments. *J. Atmos. Sci.*, **25**, 416–439.

Goff, R. C., 1976: Vertical structure of thunderstorm outflow. *Mon. Wea. Rev.*, **104**, 1429–1440.

Klemp, J. B., and R. B. Wilhelmson, 1978a: The simulation of three-dimensional convective storm dynamics. *J. Atmos. Sci.*, **35**, 1070–1096.

——, and ——, 1978b: Simulations of right and left moving storms through storm splitting. *J. Atmos. Sci.*, **35**, 1097–1100.

——, —— and P. S. Ray, 1981: Observed and numerically simulated structure of a mature supercell thunderstorm. *J. Atmos. Sci.*, **38**, 1558–1580.

Lemon, L. R., 1976: The flanking line, a severe thunderstorm intensification source. *J. Atmos. Sci.*, **33**, 686–694.

——, D. W. Burgess and R. A. Brown, 1978: Tornadic storm outflow and morphology derived from single-Doppler radar measurements. *Mon. Wea. Rev.*, **106**, 48–61.

Schlesinger, R. E., 1978: A three-dimensional numerical model of an isolated thunderstorm. Part I: Comparative experiments for variable ambient wind shear. *J. Atmos. Sci.*, **35**, 690–713.

——, 1980: A three-dimensional numerical model of an isolated thunderstorm. Part II: Dynamics of updraft splitting and mesovortex couplet evolution. *J. Atmos. Sci.*, **37**, 395–420.

Tripoli, G. J., and W. R. Cotton, 1980: A numerical investigation of several factors contributing to the observed variable intensity of deep convection over South Florida. *J. Appl. Meteor.*, **19**, 1037–1063.

Wilhelmson, R. B., and Y. Ogura, 1972: The pressure perturbation and the numerical modeling of a cloud. *J. Atmos. Sci.*, **29**, 1295–1307.

——, and J. B. Klemp, 1978: A numerical study of storm splitting that leads to long-lived storms. *J. Atmos. Sci.*, **35**, 1974–1986.